Mem. S.A.It. Vol. 84, 866

Memorie della

Formation of free-floating and companion brown dwarfs

E. I. Vorobyov[1,2] and S. Basu[3]

[1] Institute of Astrophysics, University of Vienna, Vienna, 1180, Austria
e-mail: eduard.vorobiev@univie.ac.at
[2] Research Institute of Physics, Southern Federal University, Rostov-on-Don, 344090, Russia
[3] Department of Physics and Astronomy, University of Western Ontario, London, Ontario, N6A 3K7, Canada

Abstract. The formation of brown dwarfs (BDs) is usually attributed to either of two distinct mechanisms: the direct collapse of a cloud core whose mass straddles the substellar mass limit and gravitational fragmentation in dense filaments and/or circumstellar disks, often followed by ejection of sub-stellar objects from their birth sites. It is likely that both mechanisms coexist and complement each other. However, an important argument usually in favor of the direct collapse scenario is the observation of some very-low-mass isolated proto-BD clumps, which, until recently, were difficult to explain by gravitational fragmentation. In this article, we will review the latest developments in the gravitational fragmentation scenario of BD formation. Disk fragmentation models that allow ejection of gaseous proto-BDs (and not only fully formed objects) account naturally for the formation of BD disks, avoid the problem of high ejection speeds implied in the standard ejection models of point-sized objects, and are also consistent with the observation of isolated low-mass clumps. In the ejection scenario, proto-BDs of larger masses have a higher likelihood for survival, thus providing a possible explanation for the IMF turnover at the lowmass end. Formation of wide-orbit BD companions to stars can also be explained in the disk fragmentation scenario. However, the likelihood of survival of the fragments is low, particularly at small orbital distances, which naturally accounts for the existence of the so-called BD desert.

Key words. accretion, accretion disks – brown dwarfs – hydrodynamics – instabilities – stars: formation – stars: low-mass

1. Introduction

Brown dwarfs (BDs) – enigmatic objects with masses in the $13\,M_{\rm Jup} < M_{\rm BD} < 80\,M_{\rm Jup}$ range – occupy the niche just between planets and stars and attract much interest of the astrophysical community. They have insufficient mass to burn hydrogen but they can sustain deuterium burning. They are found as companions to stars and also as isolated objects. The main question of the BD origin is whether they form as stars via direct gravitational collapse of dense cloud cores or as giant planets via disk gravitational fragmentation.

Send offprint requests to: E. I. Vorobyov

The problem with the BD origin is evident if one considers the maximum mass of an isothermal spherical cloud marginally stable against the gravitational collapse (Jeans mass)

$$M_{\rm Jeans} = \frac{4\pi^{5/3}}{24} \frac{c_{\rm s}^3}{(G^3\rho)^{1/2}}, \quad (1)$$

where $c_{\rm s}$ is the sound speed and ρ is the gas volume density. Equation (1) states that in order to form a BD with mass $< 80\,M_{\rm Jup}$ from a cloud with temperature 30 K, the required volume density has to be greater than 10^{-15} g cm^{-3} or, in terms of the corresponding number density, $n \lesssim 10^8\,{\rm cm}^{-3}$. This requirement can only be automatically fulfilled in protostellar disks with typical number densities in dense spiral arms on the order of 10^9-10^{11} cm^{-3} (Vorobyov 2010), making gravitational fragmentation of spiral arms a plausible gateway for BD formation (Stamatellos et al. 2007; Stamatellos & Whitworth 2009; Thies et al. 2010; Basu & Vorobyov 2012; Vorobyov 2013).

Typical number densities in starless cores, 10^4-10^6 cm^{-3}, imply core masses that are too high to form BDs via direct gravitational collapse. Instead, they tend to form stellar-mass objects. Therefore, several mechanisms have been proposed to circumvent this difficulty. Padoan & Nordlung (2004) suggested that colliding flows in a turbulent magnetic medium can provide the necessary compression to starless cores, pushing the gas density to a value at which the formation of BDs is enabled (see also Hennebelle & Chabrier 2008). Another possibility is that a BD is born when gravitational collapse of a stellar-mass core is modified by an additional process that prematurely halts accretion onto the forming object, such as dynamical ejection (Reipurth & Clarke 2001) or photoevaporation by ionizing radiation from massive stars (Kroupa & Bouvier 2003; Whitworth & Zinnecker 2004).

Recent numerical hydrodynamics simulations of star cluster formation can successfully reproduce the main BD characteristics such as the number of BDs relative to stars and the deficit of close-orbit BD companions (Bate 2009; Offner et al. 2009; Bate 2012). These simulations also demonstrate that the radiative feedback can largely suppress disk fragmentation, making this BD formation mechanism less efficient in comparison to that of direct gravitational collapse. In particular, Bate (2012) argues that only 1/5 of the total number of BDs is formed via disk fragmentation.

However, global simulations of star cluster formation suffer from two major caveats. First, the numerical resolution may not be sufficient to properly resolve disk fragmentation. The SPH simulations of Bate (2012) employ 35 million particles. For $\sim$ 200 resolved objects, the number of particles per a star+disk system is $\leq$ 175000. For comparison, the focused simulations of isolated disks by Stamatellos & Whitworth (2009) employed 1.0 million particles. The same lack of resolution is present in global grid-based simulations: Offner et al. (2009) had effective resolution of 4 AU, while the focused simulations of protostellar disks by Vorobyov & Basu (2010b) had resolution of $<$ 1.0 AU in the inner 100 AU of the disk.

Second, the accretion rates onto forming protostars in global simulations are usually smooth and continuous. However, there is a growing evidence from both observations and modelling that protostellar accretion can be highly variable (Kenyon & Hartmann 1995; Vorobyov & Basu 2006; Vorobyov 2009; Zhu et al. 2010; Dunham & Vorobyov 2012). Focused numerical hydrodynamics simulations of disk formation and evolution (Vorobyov & Basu 2010b) reveal that gravitationally unstable disks have accretion histories that are characterized by prolonged episodes of low-rate accretion ($10^{-8} - 10^{-6}\,M_\odot\,{\rm yr}^{-1}$) interspersed with episodic, short-lived bursts ($10^{-5} - 10^{-4}\,M_\odot\,{\rm yr}^{-1}$). As a result, stars may spend most of the early lifetime in the low-accretion (and hence low-luminosity) mode. This can facilitate disk fragmentation and formation of BDs and planets (Stamatellos et al. 2011; Vorobyov 2013).

Figure 1 illustrates the effect of variable accretion with episodic bursts. The solid line presents the total (accretion plus photospheric) luminosity of a young accreting star (the stellar mass at $t = 0.5$ Myr is $0.5\,M_\odot$) derived from focused simulations of isolated systems showing episodic accretion bursts (Vorobyov & Basu 2010b). The bursts in these simulations are triggered by disk gravitational fragmentation followed by inward migration and accretion of the fragments onto the forming protostar. The shaded area represents the range of accretion luminosity inferred from global simulation of star cluster formation with smooth accretion (figure 8 in Offner et al. 2009), assuming that the stellar mass and radius vary in the $[0.5-1.0]\,M_\odot$ and $[2-4]\,R_\odot$ limits.

The early evolution in the episodic accretion model (EAM) is characterized, in general, by much lower luminosity than that of the smooth accretion model (SAM). Luminosities in the EAM can match or exceed those of the SAM only during short luminosity outbursts. Both models tend to yield similar luminosities only in the T Tauri phase, though the EAM continues to show occasional bursts even then. The lack of accretion/luminosity variability in global star formation models is likely caused by low spatial resolution and, as a consequence, the inability to resolve disk fragmentation and physical processes leading to outbursts in the inner disk regions on sub-AU scales.

In this article, we review the latest developments in the disk fragmentation models of BD formation, which take into account episodic accretion and employ numerical resolution sufficient to resolve disk fragmentation. In Section 2, we briefly review our numerical hydrodynamics model. Section 3 discusses the formation of wide-orbit BD companions to stars (Vorobyov & Basu 2010a; Vorobyov 2013). Section 4 presents the ejection mechanism of proto-BDs (Basu & Vorobyov 2012) and Section 5 summarizes our main findings.

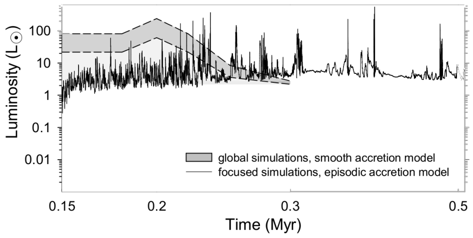

Fig. 1. Stellar luminosity vs. time in disk evolution models (solid line, Vorobyov & Basu 2010b) and global star cluster simulations (shaded area, Offner et al. 2009).

2. Model description

Our numerical model is described in detail in Vorobyov & Basu (2010b) and Vorobyov (2013), and is briefly reviewed below for the reader's convenience. We use numerical hydrodynamics simulations in the thin-disk limit to compute the gravitational collapse of starless cores. To avoid too small time steps, we introduce a "sink cell" at $r_{\rm sc} \leq 6\,$AU and impose a free boundary condition such that the matter is allowed to flow out of the computational domain into the sink cell. We monitor the gas surface density in the sink cell and when its value exceeds a critical one for the transition from isothermal to adiabatic evolution ($\sim 10^{10}\,{\rm cm}^{-3}$), we introduce a central point-mass object. The simulations continue into the embedded phase of star formation, during which a protostellar disk is formed. In this stage, the disk is subject to intense mass loading from the remnant of the parental core. The self-consistent disk-core interaction is a key feature of our model allowing us to observe repetitive episodes of disk fragmentation in some models. During the disk evolution, 90% of the gas that crosses the inner boundary is assumed to land onto the central object plus the sink cell. The other 10% of the accreted gas is assumed to be carried away with protostellar jets.

2.1. Basic equations

The basic equations of mass, momentum, and energy transport are

$$\frac{\partial \Sigma}{\partial t} = -\nabla_p \cdot \left(\Sigma \boldsymbol{v}_p\right), \tag{2}$$

$$\frac{\partial}{\partial t}\left(\Sigma \boldsymbol{v}_p\right) + \left[\nabla \cdot \left(\Sigma \boldsymbol{v_p} \otimes \boldsymbol{v}_p\right)\right]_p = -\nabla_p \mathcal{P} + \Sigma\, \boldsymbol{g}_p + (\nabla \cdot \mathbf{\Pi})_p, \tag{3}$$

$$\frac{\partial e}{\partial t} + \nabla_p \cdot \left(e \boldsymbol{v}_p\right) = -\mathcal{P}(\nabla_p \cdot \boldsymbol{v}_p) - \Lambda + \Gamma + (\nabla \boldsymbol{v})_{pp'} : \Pi_{pp'}, \tag{4}$$

where subscripts p and p' refers to the planar components (r, ϕ) in polar coordinates, Σ is the mass surface density, e is the internal energy per surface area, $\mathcal{P}$ is the vertically integrated gas pressure calculated via the ideal equation of state as $\mathcal{P} = (\gamma - 1)e$ with $\gamma = 7/5$, Z is the radially and azimuthally varying vertical scale height determined in each computational cell using an assumption of local hydrostatic equilibrium, $\boldsymbol{v}_p = v_r\hat{\boldsymbol{r}} + v_\phi\hat{\boldsymbol{\phi}}$ is the velocity in the disk plane, $\boldsymbol{g}_p = g_r\hat{\boldsymbol{r}} + g_\phi\hat{\boldsymbol{\phi}}$ is the gravitational acceleration in the disk plane, and $\nabla_p = \hat{\boldsymbol{r}}\partial/\partial r + \hat{\boldsymbol{\phi}}r^{-1}\partial/\partial\phi$ is the gradient along the planar coordinates of the disk. Turbulent viscosity is taken into account via the viscous stress tensor $\mathbf{\Pi}$. The kinematic viscosity is parameterized using the Shakura & Sunyaev α-parameterization. We use a spatially and temporally uniform α, with its value set to 5×10^{-3}. The definition of the cooling rate from the disk surface Λ and disk heating rate due to stellar and background irradiation can be found in Vorobyov & Basu (2010b).

2.2. Initial conditions in stellarless cores

In most models, the initial distribution of the gas surface density Σ and angular velocity Ω in the pre-stellar cores is taken from Basu (1997) and is typical of pre-stellar cores formed as a result of the slow expulsion of magnetic field due to ambipolar diffusion

$$\Sigma = \frac{r_0\Sigma_0}{\sqrt{r^2 + r_0^2}}\,, \tag{5}$$

$$\Omega = 2\Omega_0\left(\frac{r_0}{r}\right)^2\left[\sqrt{1 + \left(\frac{r}{r_0}\right)^2} - 1\right]. \tag{6}$$

Here, Ω_0 and Σ_0 are the angular velocity and gas surface density at the disk center and $r_0 = \sqrt{A}c_\mathrm{s}^2/\pi G\Sigma_0$ is the radius of the central plateau, where c_s is the initial sound speed in the core. The positive density-perturbation amplitude A in all models is set to 1.2.

In some models, we use the initial conditions for pre-stellar cores described by Ω=const and Σ=const, suggested by Boss & Hartmann (2001). More on the motivation and justification of the initial conditions can be found in Vorobyov (2013). Table 1 lists the main parameters of our models presented in this article.

2.3. Numerical resolution

Models presented in this article were run on a polar coordinate (r, ϕ) grid with 512×512 zones. The radial points are logarithmically spaced, with the innermost cell outside the central sink having size 0.07–0.1 AU depending on the cloud core size (i.e., the radius of the computational region). The radial and azimuthal resolution are $\lesssim$ 1.0 AU at a radial distance $r \lesssim 100$ AU.

The Truelove criterion states that the local Jeans length must be resolved by at least four numerical cells in order to correctly capture disk fragmentation (Truelove et al. 1998). The Jeans length in thin-disk models is calculated as (Vorobyov 2013)

$$R_\mathrm{J} = \frac{\langle v^2\rangle}{\pi G\Sigma_0}, \tag{7}$$

where Σ_0 is the surface density at the fragment-disk interface and $\langle v^2\rangle = 2\mathcal{R}T_0/\mu$ is the velocity dispersion of a thin disk. Fragments usually condense out of densest sections of spiral arms. The typical surface densities and temperatures in spiral arms do not exceed 100 g cm^{-2} and 100 K. Adopting these values for Σ_0 and T_0, the corresponding Jeans length becomes $R_\mathrm{J} \approx 20$ AU.

In models showing disk fragmentation, the radial and azimuthal grid resolution at $r = 100$ AU is $\approx$ 1.0 AU and the Jeans length is resolved by roughly 20 grid zones in each coordinate direction. On our logarithmically spaced radial grid, the Truelove criterion is expected to break only at $r \gtrsim 500$ AU where the grid resolution starts to exceed 5.0 AU. Fragmentation takes place mostly at radial distances from a few tens to a few hundreds AU. Fragments that are seen in our models at larger distances are most likely scattered from the inner disk regions due to gravitational interaction with other fragments.

Table 1. Model parameters.

model	M_c ($M_\odot$)	β (%)	Σ_0 (g cm^{-2})	Ω_0 (s^{-1})	r_0 (AU)
1†	1.2	0.88	1.3×10^{-2}	1.3×10^{-14}	–
2	1.7	0.56	3.3×10^{-2}	2.4×10^{-14}	3770
3	1.5	0.56	3.1×10^{-2}	2.6×10^{-14}	3430
4	1.55	1.27	3.6×10^{-2}	4.0×10^{-14}	3430
5	1.85	1.3	3.0×10^{-2}	3.8×10^{-14}	4115
6	0.85	2.25	6.6×10^{2}	9.4×10^{-14}	1885

† Models with spatially constant gas surface density $\Sigma \equiv \Sigma_0$ and angular velocity $\Omega \equiv \Omega_0$.

3. Formation of companion BDs via disk fragmentation

Focused numerical hydrodynamics simulations of massive disks around (sub)-solar-mass stars revealed the formation of multiple fragments in the BD-mass regime (e.g. Stamatellos & Whitworth 2009; Thies et al. 2010). However, these simulations, due to their three-dimensional nature, cannot follow the long-term ($\sim$ 1.0 Myr) evolution of the fragments, leaving the question of their ultimate fate uncertain. The fragments in these simulations are substituted with point-sized sink particles. When lacking the accurate thermal physics of H_2 dissociation at gas temperatures $>$ 2000 K, this procedure often results in the premature formation of BDs from fragments, which may act to overestimate the rate of BD production.

In addition, the embedded phase of star formation, where disk fragmentation predominantly takes place, presents an environment in which the survival rate of fragments is quite low. Gravitational instability is strong and resulting gravitational and tidal torques are rampant. As a consequence, part of the fragments are dispersed by the tidal torques exerted by the spiral arms (Vorobyov & Basu 2010b; Boley et al. 2010). Others are quickly driven into the disk inner regions, and probably onto the star, due to the loss of angular momentum caused by the gravitational interaction with the trailing spiral arms (Vorobyov & Basu 2006, 2010b). The net results is that disk fragmentation does *not* guarantee in the long run the survival of fragments and formation of BDs.

In our numerical hydrodynamics simulations, we therefore focus on the long-term evolution of fragments formed via disk fragmentation. We are interested in the likelihood of survival of these fragments due to either dynamical ejection from the disk, resulting in the formation of freely-floating proto-BDs, or settling on wide stable orbits, leading to the formation of wide-orbit BD companions.

Figure 2 shows a series of images of the gas surface density in model 1. The time elapsed since the formation of the central protostar is indicated in each image. This model is characterized by Σ = const and Ω = const. As a consequence, model 1 has an elevated mass infall onto the disk as compared to models with declining radial profiles of Σ.

Gravitational instability, fueled by intense mass loading from the envelope, is so strong that the disk has broken into massive clumps linked with each other by long and dense filaments. These fragments are essentially the first Larson cores— pressure and rotation supported, self-gravitating gaseous clumps with midplane temperatures $\lesssim 10^3$ K and surface densities $\lesssim 10^4$ g cm^{-2} (Vorobyov et al. 2013). During the course of the evolution, most fragments have migrated onto the star due to strong torques but one massive fragment manages to survive through the initial violent stage and settles onto a quasi-stable orbit after 0.3 Myr.

The short-lived nature of the fragments in model 1 is illustrated in Figure 3 showing the

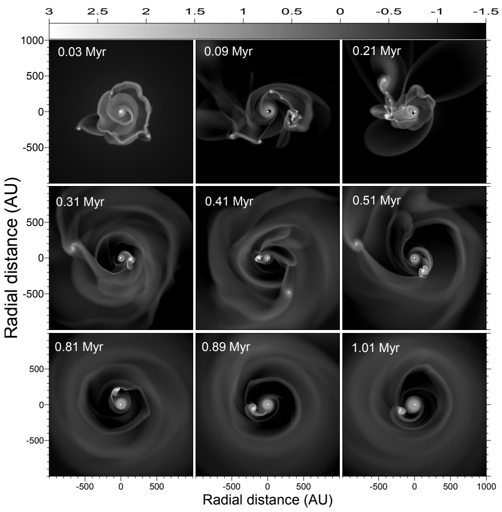

Fig. 2. Gas surface density distribution in model 1 shown at various times since the formation of the central protostar. Only the inner 2000×2000 AU box is shown, the total computational region extends to 16000 AU. The scale bar is in log g cm^{-2}. Note a fragment on a stable orbit in the bottom row.

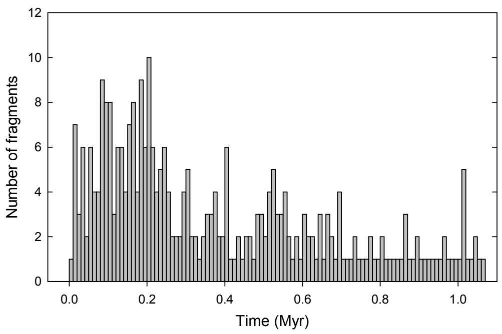

Fig. 3. Number of fragments vs. time in model 1. The number of fragments at a given time instant is calculated using the fragment tracking algorithm described in Vorobyov (2013).

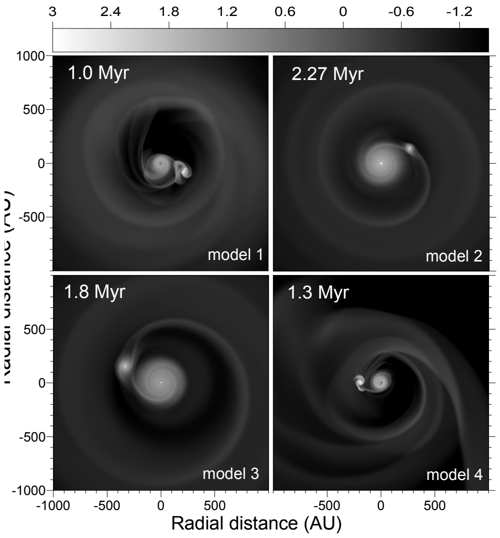

Fig. 4. Gas surface density distribution in models showing the formation of quasi-stable BD embryos on wide orbits. The model number and time elapsed since the formation of the central protostar is indicated in each panel. The scale bar is in log g cm^{-2}.

number of fragments at a given time instant. An increase in the number of fragments shows recent fragmentation, and a decrease shows recent destruction/accretion/ejection of the fragments. The maximum number of fragments $N_f = 10$ is reached at $t \approx 0.2$ Myr. Ejection of a fragment at around $t = 0.25$ Myr and the associated decline in the total disk mass weakens the disk propensity to fragment and brings the number of fragments to just a few. The subsequent episodic increases in the number of fragments reflect fragmentation that takes place in the disk of the primary fragment and/or in the filaments connecting the primary fragment with the rest of the disk, but these secondary fragments do not survive for longer than a few orbital periods and disperse presumably due to strong tidal torques exerted by the primary.

We have run 60 models with different initial masses and ratios of rotational to gravitational energy lying in the $0.1 - 2.0\,M_{\odot}$ and 0.2% – 2% limits, respectively. The total integration time in each model exceeded 1.0 Myr after the formation of the central protostar. Protostellar disks in the majority of models were sufficiently massive to experience vigorous gravitational fragmentation. The number of the fragments amounted to several (sometimes, more than 10) at a time. However, most of the fragments were either accreted by the star or were ejected from the disk or dispersed by tidal torques. Only six models out of 60 considered models revealed the survival of one of the fragments after 1.0 Myr of evolution. Four

Table 2. Characteristics of survived embryos.

model	M_* ($M_\odot$)	$\overline{M}_\mathrm{f}$ (M_J)	$\overline{M}_\mathrm{H}$ (M_J)	$\overline{r}_\mathrm{f}$ (AU)	ϵ	$\overline{R}_\mathrm{f}$ (AU)	$\overline{R}_\mathrm{H}$ (AU)
1	0.9	43	60	178	0.04	21	46
2	1.2	11	20.5	330	0.07	20	47
3	1.1	11	19	370	0.02	20.5	54
4	0.75	27.5	40.5	180	0.06	19.5	41

models produced stable proto-BD companions, while the other two produced giant planet embryos.

Figure 4 compiles four models that have demonstrated the formation of stable proto-BD companions on wide orbits, showing for each model the gas surface density image at the end of numerical simulations. The model parameters are listed in Table 1. All four BD embryos possess their own circum-embryo disks, the masses of which are comparable to those of the host. In particular, circum-embryo disks in models 1 and 4 exhibit a pronounced two-armed spiral structure.

The main characteristics of the BD embryos are listed in Table 2. In particular, columns 1–8 list the model number, mass of the protostar M_*, mean mass of the embryo $\overline{M}_\mathrm{f}$, mean mass within the Hill radius $\overline{M}_\mathrm{H}$, mean orbital distance of the embryo $\overline{r}_\mathrm{f}$, orbital eccentricity ϵ, mean radius of the embryo $\overline{R}_\mathrm{f}$, and mean Hill radius $\overline{R}_\mathrm{H}$. Several interesting conclusions drawn from Table 2 (though the statistics is rather low) will be summarized in Section 5.

4. Ejection of proto-brown dwarfs

Dynamical ejection due to many-body gravitational interactions has been suggested as a possible gateway for the BD formation (Reipurth & Clarke 2001; Stamatellos & Whitworth 2009; Bate 2009). However, the use of sink particles in numerical simulations can not only overestimate the number of BDs but also introduce the uncertainty in the ejection efficiency due to freedom in the definition of the smoothing length of gravitational interaction of point-sized objects. Numerical modeling that is free from sink particles can give us important information on the efficiency of ejection of proto-BD embryos (Basu & Vorobyov 2012). Below we provide two prototype examples.

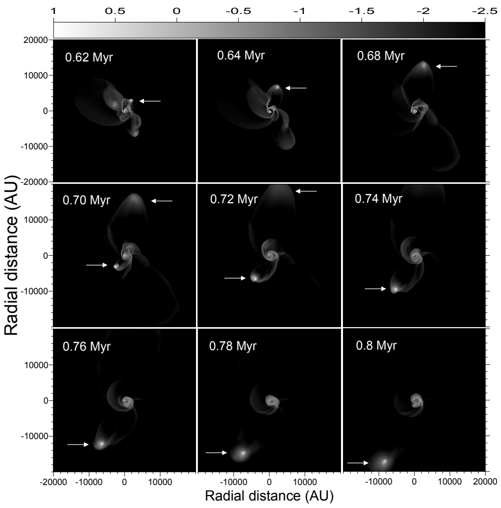

Fig. 5. Gas surface density distribution (g cm^{-2}, log units) in model 5 at several time instances after the formation of a central star. Arrows identify clumps that are ejected from the system after a multi-body interaction within the centrifugal disk.

Figure 5 shows a sequence of column density images for model 5 capturing two ejection events in a region of size 2×10^4 AU on each side. Arrows in the images identify the two ejected fragments. The first ejection takes place at $\approx$ 0.6 Myr after the formation of the central protostar. The ejected fragment is surrounded by a nebulosity and is connected with the parental disk by a low-density gaseous tail. The mass of the fragment is $\approx 0.04\,M_\odot$ and the mass within the Hill radius is ≈ 0.07 $M_\odot$. The ejection speed (∼ 0.75 km s^{-1}) is nearly twice greater than the escape speed. As the fragment moves nearly radially outward, it grows in size and finally disperses before leaving the computational box. This effect may be an artifact of the decreasing resolution of our numerical grid at larger radii, but it may also be caused by tidal perturbation during the close encounter in the inner part of the disk.

The second ejection takes place at ≈ 0.69 Myr. The fragment survives through the entire journey to the outer computational boundary. The mass of the second ejected fragment is ≈ 0.12 $M_\odot$ and the mass within the Hill radius is ≈ 0.2 $M_\odot$. The ejection speed (≈ 0.5 km s^{-1}) is twice greater than the escape speed. This fragment can ultimately form a very-low-mass star with a rather massive disk.

Figure 6 illustrates the successful ejection of a proto-BD embryo in model 6. Soon after leaving the parental disk, the fragment breaks into a pair of smaller fragments (this occurs at t ≈ 0.5 Myr). The least massive of the two ultimately disperses, contributing its gas reservoir to a massive and extended disk around the more massive counterpart. The mass of the survived fragment is ≈ 0.05 $M_\odot$ and the mass within the Hill radius is ≈ 0.09 $M_\odot$. The ejection speed, ∼ 0.45 km s^{-1}, is 1.5 times greater than the escape speed. This example shows that the ejection of BD-BD pairs is in principle possible, though future higher resolution simulations will be needed to verify this phenomenon.

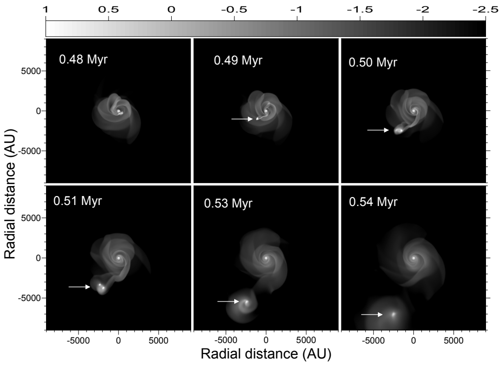

Fig. 6. Gas surface density images (g cm^{-2}, log units) in model 6 showing the ejection of a proto-BD (marked by arrows).

5. Conclusions

Numerical hydrodynamics simulations in the thin-disk limit allow us to study the formation and long-term evolution of circumstellar disks around (sub-)solar mass stars. Disk gravitational fragmentation can be adequately resolved and studied without resorting to the use of sink particles (Vorobyov & Basu 2010b).

Our models reveal the formation of multiple gaseous self-gravitating fragments in the disk, most of which end up spiralling into the forming star. A few fragments may be ejected from the disk via many-body gravitational interactions (Basu & Vorobyov 2012). Our results support a new hybrid paradigm of BD and low-mass star (LMS) formation by disk fragmentation followed by fragment ejection (rather than by ejection of fully formed low-mass stars/BDs). We speculate that these proto-BD embryos will ultimately evolve, upon cooling and contraction, into freely floating, isolated BDs or low-mass stars.

The main conclusions from this scenario can be summarized as follows.

- The ejected proto-BDs often host rotationally supported envelopes/disks, which can naturally account for the presence of disks around fully formed BDs.
- Relatively low ejection speeds obtained during close encounters of AU-sized fragments (rather than point-sized sink particles) can account for the observed velocity dispersion and physical location of BDs relative to young stars.
- Ejected fragments can explain the existence of isolated proto-BD cores.
- Reduced efficiency of ejection of low-mass fragments (due to possible tidal dispersal) can account for the IMF turnover in the BD mass regime.
- The number of ejected BD embryos is ∼ 1 − 2 during the lifetime of a fragmentationally unstable disk.

In rare events, a fragment may settle onto a stable, wide-separation orbit, giving birth to a proto-BD companion to a (sub-)solar mass star

(Vorobyov & Basu 2010a; Vorobyov 2013). Several interesting conclusions can be drawn from our modeling.

- Disk fragmentation can account for the formation of low- to intermediate-mass BD companions in the 13–43 $M_{\rm Jup}$ range. It appears that protostellar disks are not massive enough to form the upper-mass BD companions.
- Disk fragmentation accounts for the formation of BD companions at orbital distances 150–450 AU. Objects at smaller distances are torqued onto the star by the gravitational interaction with spiral arms, leading to the formation of the so-called BD desert. Very wide separation BD companions (> 500 AU) are likely to form via core fragmentation or gravitational capturing, because protostellar disks rarely exceed several hundred AU in radius (Vorobyov 2011).
- Disk fragmentation cannot account for the formation of BD companions to low-mass stars with mass $\lesssim 0.7\,M_\odot$, most likely because these stars cannot sustain circumstellar disks that are sufficiently massive to experience gravitational fragmentation.
- The overall low probability for the formation of BD companions to stars via disk fragmentation (~ 10%) is in general agreement with a low number of such objects.

While disk fragmentation seems to explain the whole mass range of observed wide orbit companions, it has difficulty with explaining companions at extremely wide orbits (~ 1000 AU) around low-mass ($\leq 0.7\,M_\odot$) stars as observed, e.g., in the TMR-1 system (Riaz et al. 2013).

Acknowledgements. E.I.V. acknowledges support from the RFBR grant 11-02-92601-KO. The simulations were performed on the SHARCNET, ACEnet, and VSC-2 Scientific clusters. S. B. acknowledges support from an NSERC Discovery Grant.

References

Basu, S. 1997, ApJ, 485, 240
Basu, S., & Vorobyov, E. I. 2012, ApJ, 750, 30
Bate, M. 2009, MNRAS, 392, 590
Bate, M. 2012, MNRAS, 419, 3115
Boley, A. C., Hayfield, T., Mayer, L., & Durisen, R. H. 2010, Icarus, 207, 509
Boss, A. P., & Hartmann, L. W. 2001, ApJ, 562, 842
Dunham, M. M., & Vorobyov, E. I. 2012, ApJ, 747, 52
Hennebelle, P., & Chabrier, G. 2008, ApJ, 684, 395
Kenyon, S. J., & Hartmann, L. 1995, ApJS, 101, 117
Kroupa, P., & Bouvier, J. 2003, MNRAS, 346, 369
Offner, S. S. R., Klein, R. I., McKee, C. F., Krumholz, M. R. 2009, ApJ, 703, 131
Padoan, P., & Nordlund, A. 2004, ApJ, 617, 559
Reipurth, B., & Clarke, C. 2001, AJ, 122, 432
Riaz, B., Martín, E. L., Petr-Gotzens, M. G., & Monin, J.-L. 2013, arXiv:1306.5271
Stamatellos, D., Hubber, D. A., & Whitworth, A. P. 2007, MNRAS, 382, L30
Stamatellos, D., & Whitworth, A. P. 2009, MNRAS, 392, 413
Stamatellos, D., Whitworth, A. P., & Hubber, D. A. 2011, ApJ, 730, 32
Thies, I., Kroupa, P., Goodwin, S. P., Stamatellos, D., & Whitworth, A. P. 2010, ApJ, 717, 577
Truelove, J. K., Klein, R. I., McKee, C. F., et al. 1998, ApJ, 495, 821
Vorobyov, E. I. 2009, ApJ, 704, 715
Vorobyov, E. I. 2010, ApJ, 723, 1294
Vorobyov, E. I. 2011, ApJ, 729, 146
Vorobyov, E. I. 2013, A&A, 552, 129
Vorobyov, E. I., & Basu, S. 2006, ApJ, 650, 956
Vorobyov, E. I., & Basu, S. 2010a, ApJ, 714, L133
Vorobyov E. I., & Basu S. 2010b, ApJ, 719, 1896
Vorobyov, E. I., Zakhozhay, O. V., & Dunham, M. M. 2013, MNRAS, 433, 3256
Whitworth, A. P., & Zinnecker H. 2004, A&A, 427, 299
Zhu, Z., Hartmann, L., & Gammie, C. 2010, ApJ, 713, 1143